STRUCTURE OF THE MAGNETOPAUSE BOUNDARY LAYERS DISCOVERED BY CLUSTER MULTIPOINT OBSERVATIONS

Hiroshi Hasegawa

Department of Earth and Planetary Sciences, Tokyo Institute of Technology, 2-12-1 Ookayama, Meguro, Tokyo 152-8551, Japan, Email: hase@worldp.net

ABSTRACT

The Cluster spacecraft, when their separation is of the order of thousand km, have provided an opportunity to unveil details of complex, meso-scale structures embedded in and near the magnetopause. In this paper, we show some examples of how model-based data analyses help us to interpret data obtained by the multi-point measurements. For example, unambiguous identification of highly rolled-up Kelvin-Helmholtz vortices at the flank magnetopause, which can be the agent for efficient transport of solar wind plasmas into the magnetosphere, has been made possible with the help of three-dimensional magnetohydrodynamic simulations optimized for the magnetotail flank situations. On the other hand, two-dimensional (2D) structures of the magnetopause and of flux transfer events and their time evolution have been revealed thanks to the application of Grad-Shafranov reconstruction technique, a model-based data analysis method to produce a 2D map of the magnetic field around the spacecraft trajectory, to the Cluster data.

1. INTRODUCTION

The Cluster spacecraft have undoubtedly provided us the possibility of studying space plasma phenomena/structures in and around the Earth's magnetosphere from a three-dimensional (3D) point of view. However, it has still been difficult to gain information useful for their understanding from in situ measurements at four points only. Observing the magnetosphere, which is now well recognized to have highly 3D and dynamical aspects, with four satellites is similar to a situation in which we have access to data obtained at only four grid points in a large-scale 3D numerical simulation domain.

In such a situation, some hints from theoretical models should be helpful for us to interpret spacecraft data. These models, by necessity, involve some assumptions or approximations which may not exactly be applicable to real situations that are always highly complex, but give some important insights into what should be seen in the data when something predicted from the models is happening. In the present paper, we show how a combination of the Cluster coordinated multipoint measurements and theoretical models has enabled us to discover, and to study in detail, structures embedded in and near the magnetopause, such as flux transfer events (FTEs) [1] and vortices developed through the Kelvin-Helmholtz instability (KHI) (e.g., [2]).

We first show that unambiguous identification of highly rolled-up KH vortices at the dusk flank magnetopause [3] has been achieved by a combination of Cluster and realistic 3D magnetohydrodynamic (MHD) simulations of the KHI. We also show that there is an indicator of fully rolled-up KH vortices, which can be identified even by single-spacecraft observations. It should be emphasized that this indicator has been found through a simulation study of the KHI.

Next, we present 2D structures of the magnetopause and FTE that have emerged through a combination of Cluster and Grad-Shafranov reconstruction, a model-based data analysis method for the creation of a 2D map of magnetic field structures in space by use of in situ spacecraft measurements. The reconstruction results demonstrate time evolution of the magnetopause structure, and give information about appropriate FTE models, the orientation and scale size of FTEs, and the nature of magnetopause reconnection, such as component or anti-parallel merging and the reconnection rate.

2. DETECTION OF ROLLED-UP KELVIN-HELMHOLTZ VORTICES

2.1 Expectation from numerical simulations

The mechanisms by which solar wind plasmas are transported into the magnetosphere, in particular, during northward interplanetary magnetic field (IMF) periods when magnetic reconnection should be less efficient at the low-latitude magnetopause, have long been a focus of debate. The low-latitude boundary layer [4], in which the solar wind and magnetospheric plasmas coexist, becomes thicker and the plasma sheet on the night side becomes cooler and denser for northward IMF than for southward IMF (e.g., [5-7]), indicating that significant entry of solar wind plasmas occurs under northward IMF conditions as well. The Kelvin-Helmholtz instability (KHI) that can grow along the

flank magnetopause, across which a substantial velocity shear exists, has been proposed as a candidate mechanism for plasma transport under such conditions (e.g., [8]). Recent numerical simulations interestingly show that transport of plasma is inevitable in a highly rolled-up vortex created in the nonlinear phase of the KHI. According to these studies, plasma transport across the magnetopause can be accomplished through reconnection or turbulence induced in the rolled-up vortex [9-11], or through collapse of the vortex mediated by electron inertia effects [12]. When vortical plasma flows, generated through the nonlinear development of the KHI, can overcome the magnetic tension, the field lines in the vortex may be twisted into an anti-parallel geometry and be reconnected, resulting in field-aligned entry of solar wind plasmas through the interconnected field lines. On the other hand, the Rayleigh-Taylor (RT) instability may be triggered in a rolled-up vortex, because centrifugal force operating on plasmas rotating in the vortex can be regarded as an effective gravity and the interface between dense and tenuous plasmas in the vortex can become RT unstable. According to a simulation study [11], this RT instability in the vortex leads to a highly turbulent state. Reference [12] suggests that secondary KHI can be excited within a rolled-up vortex because, in the presence of finite electron inertia effects, a current-driven instability starts to grow in the nonlinear stage of the KHI and provides seed perturbations for the secondary KHI. Consequently, the parent, MHD-scale vortex collapses, resulting in intermixing of two plasmas that were originally separated by the velocity shear layer.

In fact, the tail flank of the magnetosphere has a highly 3D geometry, with the plasma sheet that can become KH-unstable being sandwiched between the KH-stable northern and southern lobes (see Fig. 1a). Whether or not the KHI can grow vigorously enough to form a rolled-up vortex in such a situation is not a straightforward question. To address this issue, Reference [13] has conducted 3D MHD simulations of the KHI under the magnetotail flank-like situation and have shown that a KH vortex can be fully rolled-up as long as the thickness of the plasma sheet is comparable to, or larger than, the KHI wavelength (3 to 9 R_E) [3,15] and the magnetic field component in the direction along the shear flow is sufficiently small.

Quasi-periodic perturbations in plasma and magnetic field parameters or multiple crossings of the magnetopause have often been observed by spacecraft located near the flank magnetopause and are often interpreted as being associated with surface waves or vortices excited by the KHI (e.g., [14-16]). However it was not possible from these single- (or dual-) spacecraft measurements to conclude with certainty whether those perturbations were due to the rolled-up vortices, the vital ingredient for plasma to be transported, or just to small-amplitude surface waves that do not seem to transport plasma.

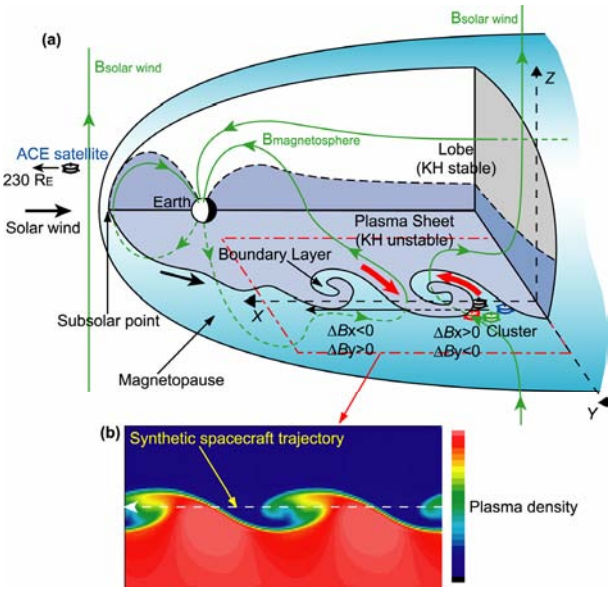

Fig. 1. Three-dimensional (3D) cutaway view of the magnetosphere showing signatures of the Kelvin-Helmholtz instability (KHI). (a) View of the magnetosphere showing the KH vortices excited along the duskside magnetopause. The KHI can grow at the interface between the solar wind and the plasma sheet in both of which the plasma energy dominates, whereas it cannot grow at the interface between the solar wind and the lobes where the magnetic energy dominates and the magnetic tension prevents it from deforming the magnetopause. Consequently, the vortices can evolve only along the low-latitude magnetopause and only low-latitude portions of the magnetospheric and solar-wind field lines are entrained into the vortices, inducing characteristic field perturbations in regions off the equator. The coordinate system is defined such that $-x$ is in the direction of motion of the vortex structure which was sliding anti-sunward in the spacecraft frame, y points outward along the magnetopause normal, and z points to the north. (b) Vortex structure resulting from a 3D numerical simulation of the magnetohydrodynamic KHI in a magnetotail flank-like geometry. Colour-coded is the plasma density in an x-y cross-section cut below the equatorial plane. The density, velocity, and magnetic field variations predicted from the simulation along a synthetic satellite trajectory denoted by the white dashed line are shown in Fig. 2.

2.2 Cluster observation of rolled-up vortices

In this subsection, we show that the unambiguous presence of rolled-up KH vortices at the magnetopause has been confirmed thanks to multipoint measurements by the four Cluster spacecraft [3]. Fig. 2 shows the Cluster observations made during the interval 20:26-20:42 UT on 20 November, 2001, when the spacecraft resided in the dusk flank magnetosphere just behind the dawn-dusk terminator (The GSM position of Cluster was (x, y, z) ~ (–3, 19, –3) R_E). The spacecraft were separated by about 2000 km from each other. The IMF seen by the ACE spacecraft, located near the L1 point 230 R_E upstream of the Earth, was northward for more than 14 hours on this day. It indicates that the upstream condition was suitable for the KHI to grow [17], but was not suitable for magnetopause reconnection to occur, at the location of Cluster (Fig. 2g). As seen in Fig. 2, Cluster observed quasi-periodic perturbations in all plasma and magnetic field parameters, which have a

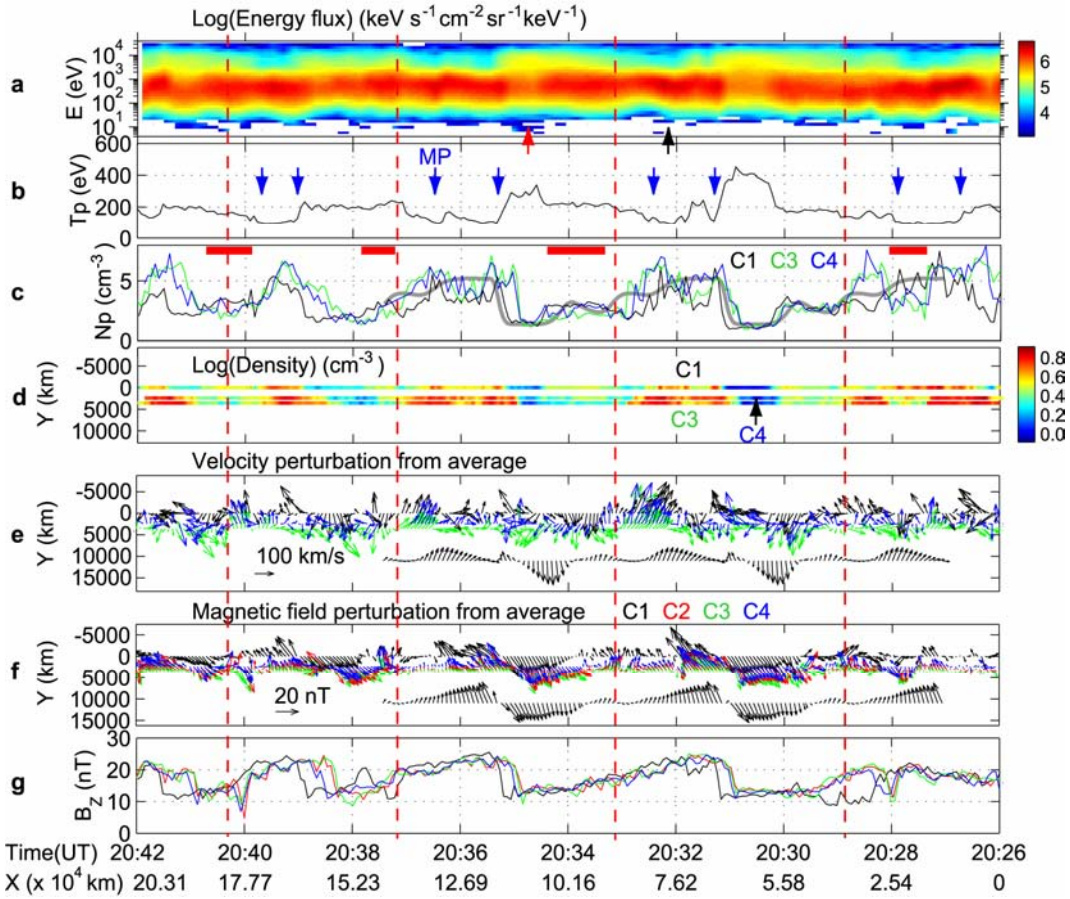

Fig. 2. Detection by Cluster of rolled-up plasma vortices on 20 November 2001 (20:26-20:42 UT). (a) The omni-directional energy spectrogram of ions observed by the Cluster 1 spacecraft (C1). Time progresses to the left and is translated into the position of the spacecraft as follows. In Earth's rest frame, the spacecraft motion is neglected as compared to that of the vortices. $-x$ is in the direction of the vortex motion in the spacecraft frame. The vortex velocity, V_{mean}, is computed by averaging the ion bulk velocity vectors measured by C1, C3, and C4 over the above interval. The spacecraft position is determined using an equation, $x = |V_{mean}|\ t + \Delta x_{i1}$, where t is time elapsed from the start of the interval, and Δx_{i1} is the x position of the i-th spacecraft relative to C1. The arrows at the bottom denote the moments when the ion velocity distributions shown in Fig. 3 were observed. (b) The ion temperature measured by C1. The blue arrows mark approximate locations of the magnetopause. (c) The plasma density variations, which are similar to those predicted by the numerical simulation (thick grey curve). Red bars indicate instances when C1 observed higher density than C3 and C4. (d) The plasma density colour-coded and projected along the spacecraft trajectories. y is orthogonal to both x and the direction of the averaged magnetic field, B_{mean}, and points outward along the magnetopause normal. (e), (f) The x-y projection of the velocity and magnetic field deviations from V_{mean} and B_{mean}, respectively (C1:black, C2:red, C3:green, and C4:blue), along with the behaviour predicted by the simulation (below). The red dashed vertical lines mark the approximate centres of the vortices. The spacecraft separation distance and the length of the arrows are doubled in the y direction. (g), The z component of the measured magnetic field.

period of 2-4 minutes. The density shown in Fig. 2c shows strong up and down variations, indicating that the spacecraft was moving back and forth between the magnetosheath and the magnetosphere. These features suggest that the magnetopause surface was corrugated, implying the excitation of the KHI at the boundary during the interval.

To see if rolled-up KH vortices were involved in this observation, here we describe, according to a simulation result, what should be expected within a rolled-up vortex. Since a considerable plasma density gradient exists across the magnetopause, the vortical plasma flow, which is a well-known feature present in the nonlinear phase of the KHI, leads to a peculiar density structure in a KH vortex. As eddy turnover proceeds, the dense, magnetosheath plasma intrudes into the magnetosphere from the anti-sunward edge of the KH waves, and results in a filament-like high-density region sitting on the magnetospheric side of tenuous plasma (Fig 1b).

This reversed density structure as well as the vortical plasma flow pattern has indeed been identified by Cluster (Fig. 2d, e). For the intervals marked by the red line segments in Fig 2c, Cluster 1 (C1) located on the most magnetospheric side observed plasmas which are denser than those seen by C3 and C4 located on the magnetosheath side of C1. This fact demonstrates that overturning of KH waves was occurring in this event. In addition, the density variation seen by C1 agrees well with that predicted from the simulation along a synthetic spacecraft trajectory that passes through the centre of rolled-up vortices (Fig. 2c). This suggests that Cluster was moving through the central portion of the vortices from their tailward side toward the sun. Since the spacecraft should in fact have been nearly at rest in the Earth's rest frame, it turns out that the vortices were convected tailward along the magnetopause at a speed of about 210 km/s, which has been estimated by averaging the velocity vectors measured by C1, C3, and C4, over the interval under discussion. Fig. 2e shows that the velocity perturbation vectors, transformed into the frame of the vortices and viewed from the north, change its orientation in a counter-clockwise sense around the centre of the vortices. This sense of rotation is precisely consistent with that expected in a vortex excited at the duskside magnetopause. These facts indicate that Cluster did encounter rolled-up KH vortices.

One may see that the measured velocity fluctuations are highly perturbed and do not agree well with those predicted from the simulation. However it should be noted that there are several effects that could lead to this discrepancy. First, the orientation of the flow perturbations may differ, depending on which part of the rolled-up, filamentary density structure the spacecraft were observing. The predicted vectors, shown in Fig. 2e, should be seen only along the trajectory penetrating through the exact centre of the vortices. If the actual spacecraft trajectory is somewhat shifted from the centre, it may see flow perturbations with different orientations (the exact location of the spacecraft relative to the vortex centre is hardly known from the measurements). Second, seed velocity fluctuations present in space, which would have initiated the KHI perhaps on the front side of the magnetosphere, would not be organized at all as in the simulation, but should have had various orientations and magnitudes. This may lead to more complex flow perturbations in the real vortices than seen in the simulation. Third, in a highly rolled-up vortex, secondary instabilities as predicted in [11,12] could be triggered and, as a result, smaller scale vortices develop, resulting in strongly complex plasma flows within the large-scale vortex. If this is the case, the less organized flow perturbations seen in the observation are consistent with the view that plasma transport, evidence of which will be given in the next subsection, occurred via the secondary instabilities excited in the discovered large-scale vortices. Fourth, the spatial dimension of the magnetosphere in the direction along the solar wind (shear) flow is much larger than the wavelength of fastest growing KH mode [18]. In such a situation, two or more vortices may coalesce to form one larger vortex. If the measurement was made during the phase of the coalescence, it is quite possible that flow perturbations in the vortices are highly variable.

In addition to the above plasma signatures of the KH vortices that appear in both 2D and 3D situations, a characteristic magnetic field perturbation pattern that should manifest only in a 3D configuration of the tail flank was identified by Cluster (Fig. 2f). This field perturbation, first predicted by 3D MHD simulations [13], can be induced in near-magnetopause regions between the plasma sheet and the lobes, because the KHI develops only along the plasma sheet-magnetosheath interface and only low-latitude portions of the near-magnetopause field lines are pulled into the vortices (Fig. 1a). Cluster situated on the southward side of the equatorial plane successfully detected bipolar signatures expected on this side in the x and y magnetic field components, in correlation with the density variation, when it crossed the trailing edge of the KH waves [3]. This combined plasma and magnetic field observations demonstrate that the roll-up of KH vortices occurred at the magnetopause under a 3D configuration of the magnetosphere.

2.3 Implications for boundary layer formation

Cluster detected cool ions of magnetosheath origin on the magnetospheric side of the magnetopause and, importantly, in the vicinity of the rolled-up vortices. As seen in Fig. 2a, the low-energy ions of magnetosheath origin are found throughout the relevant interval, even in the lowest density region corresponding to the

magnetosphere. Consistently, the ion temperature in the magnetosphere is seen to be low as compared to its typical value (Fig. 2b), because of the existence of the cool, magnetosheath ions. The top and bottom panels of Fig. 3 show examples of ion velocity distributions seen on the magnetosheath and magnetospheric sides, respectively, of the magnetopause. The latter distribution clearly shows that cool, magnetosheath-like ions coexist with the hot, magnetospheric ions. These facts are consistent with the prediction that the magnetosheath plasma is transported across the boundary as a consequence of the nonlinear growth of the KHI.

One can roughly estimate the thickness of the boundary layer that could result from the KHI, by comparing the observation and numerical simulation results. Numerical simulations show that the width of a highly rolled-up KH vortex, which would be equivalent to that of the plasma mixing layer, reaches about a half of the wavelength of one vortex (see the bottom panel of Fig. 4). (Note that the vortex in Fig. 1b is flattened because of the 3D KHI effect and because the cut is obtained at an off-equator region.) The wavelength estimated from the measurement is 6-9 R_E, the value obtained by multiplying the streaming speed of the vortices (210 km/s) and the period of quasi-periodic perturbations associated with the KH waves (3-4 minutes). We can thus infer that the boundary layer with the thickness of 3 to 4 R_E had been formed in the most KH-unstable low-latitude regions near, or at least further downstream of, the observation site. The fact that Cluster remained in the boundary layer for more than 13 hours on the day is consistent with the existence of such a thick boundary layer. It must be pointed out that the position of Cluster when it detected the vortices was just behind the dawn-dusk terminator (x~ –3 R_E). Therefore we can reasonably expect more severe development of the KHI and coalescence of two or more vortices in regions further downstream of the spacecraft. If this was truly happening, the thickness of the mixing layer in such regions must have been much larger than the estimated value of 3-4 R_E, which should be significant in terms of the formation of the tail boundary layer.

Under the 3D KHI effects, the twisting of the magnetic field lines may lead to a fairly anti-parallel configuration of the magnetosheath and geomagnetic field lines at the trailing edge of the KH waves, in regions between the plasma sheet and the lobes. A larger magnetic shear was indeed observed at the trailing edge (the shear at the edge was about 70^o while it was less than 10^o elsewhere). In addition, a thin magnetopause current sheet, an important element for the triggering of reconnection, may be formed exactly in such a region because the current sheet is compressed from both sides of the boundary owing to vortical plasma motion [12]. It is therefore quite likely that magnetopause reconnection is facilitated near the vortices as a consequence of the KHI development. Then one can easily expect efficient entry of solar wind plasmas onto magnetospheric field lines. But the present plasma measurements are not sufficient to resolve such fine-scale processes, and identification of the exact microphysical transport mechanism embedded in the vortices may await future spacecraft missions such as MMS-SMART and Cross-Scale.

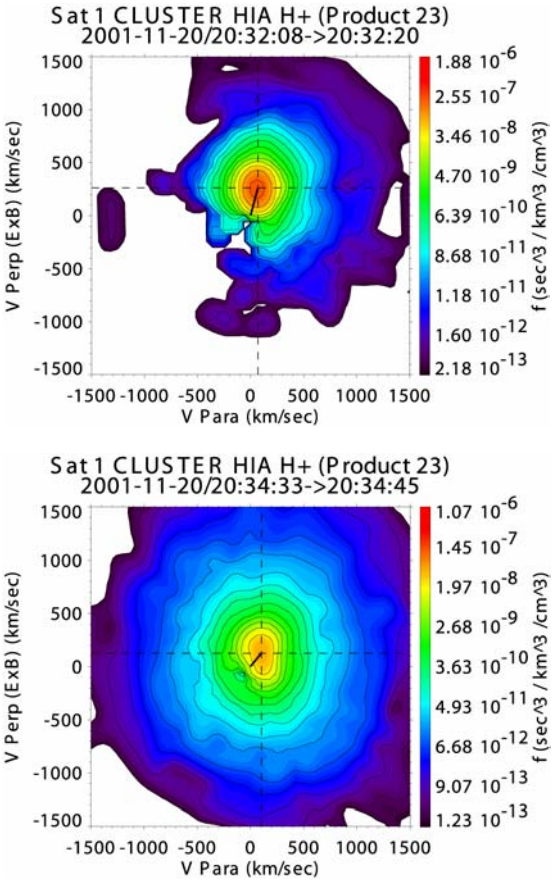

Fig. 3. Ion velocity distributions observed by C1, cut by the plane that contains the measured magnetic field (aligned with the horizontal axis) and bulk velocity (shown as a black line segment with its root at the centre) vectors. The top panel shows the distribution seen in the magnetosheath, sampled at 20:32:15 UT which is marked by the black arrow in Fig. 2a, while the bottom panel shows the distribution in the magnetosphere but in the vicinity of the vortices, sampled at 20:34:40 UT marked by the red arrow. The latter clearly shows the coexistence of cold, magnetosheath and hot, magnetospheric ion populations, suggesting that plasma transport across the boundary occurred in association with the KHI.

2.4 Single-spacecraft detection of roll-up possible?

Since we now appreciate that rolled-up vortices are an important ingredient for plasma transport via the KHI to occur and that the roll-up of KH vortices can indeed occur along the flank magnetopause, it is natural for us to attempt to find if there is some indicator of the roll-up that can be identified even in single-spacecraft observations. For this purpose, we inspect if there is any clear difference between rolled-up and not-rolled-up vortices seen in a 3D MHD simulation of the KHI. Fig. 4 shows simulation results at the moment the growth of the KHI has just saturated. In the left panels, the density in the most KH unstable plane is represented as colour contour, for three different initial conditions. These panels indicate, from top to bottom, that a KH wave is not-rolled-up, weakly-rolled-up, and fully-rolled-up, respectively. The right panels show corresponding scatter plots, constructed from the simulated data, in which the x (along the initial velocity shear) component of the flow velocity is plotted against the plasma density. Here the data points are sampled equally from a simulation domain surrounding the KH wave. One should thus expect this kind of relationship between V_x and the density to be seen, if spacecraft uniformly observes the region in the vicinity of a KH wave. What is important and interesting here is that, in the fully-rolled-up case, some fractions of the low-density, magnetospheric plasmas are flowing faster, in the $-x$ (anti-sunward) direction, than the dense, magnetosheath plasma (which has the velocity of $-1\cdot(0.5V_0)$ and the density of unity in the plot). In the not- or weakly-rolled-up cases, on the other hand, the scatter plots only show a monotonous profile with no low-density and higher-speed flow.

This anti-sunward acceleration of the low-density plasma is explained by the force balance in a rolled-up vortex in the direction radial from the centre of the vortex. Since at a certain radial distance the centrifugal force operating on denser and tenuous fluids must be equal, the tenuous, magnetospheric plasma must rotate faster than the denser, magnetosheath plasma in the vortex [12].

To see whether or not this "low-density and higher-speed" feature can be used as an indicator of the roll-up, we show in Fig. 5 a scatter plot of the x component of the bulk velocity and ion density, constructed using the data obtained during the interval when Cluster detected the rolled-up KH vortices [3]. The plot indeed shows the presence of low-density ions that are streaming anti-sunward with a speed higher than the magnetosheath ions. While the anti-sunward speed of the densest, magnetosheath ions was about 250 km/s, that of less dense (< 5 /cc) ions reaches up to 350 km/s.

Since a scatter plot as shown in Fig. 5 can easily be produced and the "low-density and higher-speed" feature can easily be identified even from single-spacecraft data, our finding suggests that single-spacecraft detection of rolled-up vortices is now possible. Of course, the signature solely must not be taken as the smoking gun evidence of the roll-up, since such a low-density and high-speed flow may be produced also as a result of magnetopause reconnection or of time-varying solar wind conditions. We emphasize that the above signature must be found together with other signatures of the KHI, to conclude with certainty that vortices are rolled-up. Such signatures that can be identified even with single-spacecraft observations would be quasi-periodic perturbations in the plasma and magnetic parameters and vortex-like flow fluctuations.

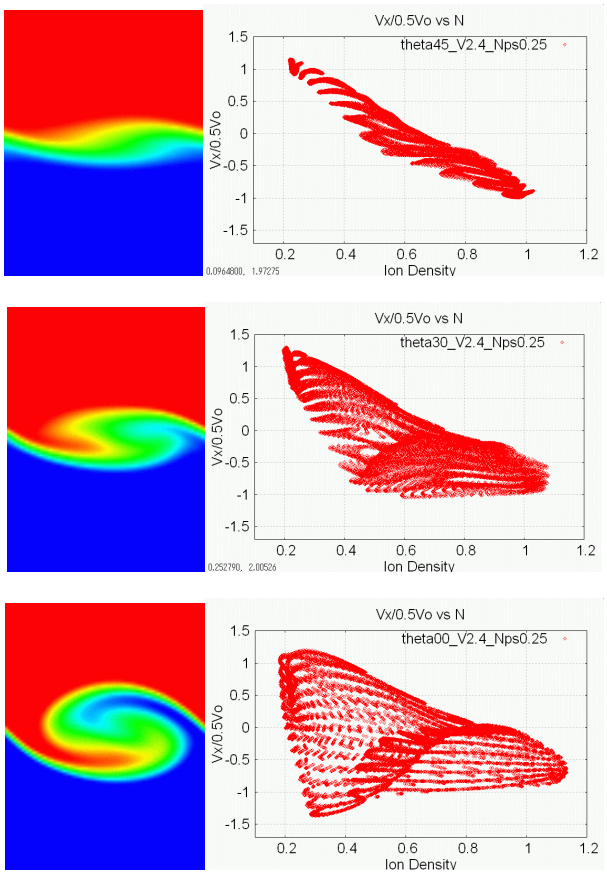

Fig. 4. Difference between "rolled-up" and "not-rolled-up" vortices. The left panels show the density in the x-y plane in colour while the right panels show scatter plots of V_x and density, constructed using data from a simulation domain that covers the KH wave/vortex. The top to bottom panels represent not-rolled-up, weakly-rolled-up, and fully-rolled-up vortices, respectively.

It is noted that the above indicator of the roll-up can be used to survey rolled-up vortices from data obtained by past single-spacecraft observations. Such a survey would permit us to investigate the occurrence probability of rolled-up vortices and even the conditions under which KH waves can be rolled-up. Furthermore, the result implies that, when the spacecraft separation of Cluster is small, the detection of rolled-up KH vortices can be made by any of the four spacecraft by identifying the "low-density and higher-speed" flows along with other KH-associated signatures. Then its coordinated multipoint measurements can be used to investigate in detail the properties of small-scale waves excited, or of thin current sheets formed, in the vortex. Interestingly, Reference [19] has recently discovered, in the polar cusp, small-scale coherent vortices as a manifestation of Alfvénic turbulence, when the Cluster separation was about 100 km. It should be mentioned that this kind of study is now possible for rolled-up vortices as well, i.e., small-scale physics embedded in the large-scale rolled-up vortices can be studied with Cluster. As a result, we may be able to gain some information about connections between macro-scale KH vortices and micro-scale phenomena/structures. Such should be a future direction to establish the ultimate plasma transport mechanism operating in the vortices.

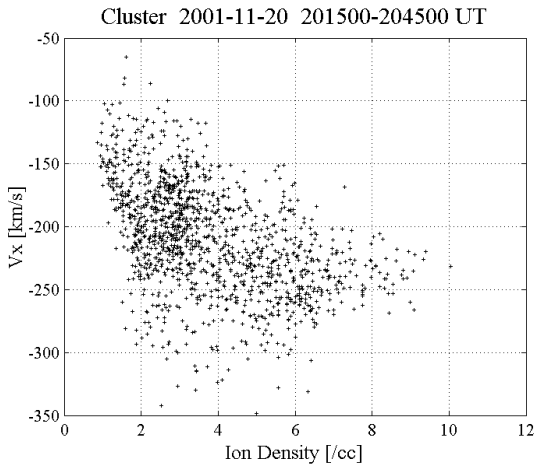

Fig. 5. Scatter plot of the x component of the bulk velocity and plasma density, constructed using the data obtained by Cluster during the interval (20:15-20:45 UT) when rolled-up KH vortices were identified with multipoint measurements. The x component represents the one tangential to the unperturbed magnetopause surface and directed sunward.

3. 2-D STRUCTURE OF THE MAGNETOPAUSE AND FLUX TRANSFER EVENT

3.1 Grad-Shafranov reconstruction

Grad-Shafranov (GS) reconstruction technique is a data analysis method which generates a 2D map of magnetic field and plasma structures from spacecraft measurements. The original version of the method produces a field map from single-spacecraft data [20]. The underlying assumptions are as follows: (1) as seen in a frame moving with the structure, which is usually taken as the deHoffmann-Teller (HT) frame [21], the structure is approximately time-stationary. In this HT frame, the plasma flow is as nearly field aligned as the velocities and magnetic fields, measured during the event, permit. (2) Inertia effects are negligible, reducing the MHD equation of motion to the equation, $j \times B = \nabla p$, representing the balance between force from the gradient of the total (thermal plus magnetic) pressure and magnetic tension. This is the case if the plasma velocities in the HT frame are small compared to the Alfvén speed and the sound speed, but also for larger field-aligned plasma speeds, if the field magnitude variations along field lines and the field-line curvature (and hence the streamline curvature) are small. The structure can then be considered magnetohydrostatic. (3) The structure is elongated in some, initially unknown, direction, z, which we refer to as the invariant axis. The assumption $\partial/\partial z = 0$ is then adopted so that the structures we recover will be 2.5 dimensional. As a result, the above force balance equation is further reduced to the so-called GS equation in the (x, y, z) Cartesian coordinate system (e.g., [22]):

$$\frac{\partial^2 A}{\partial x^2} + \frac{\partial^2 A}{\partial y^2} = -\mu_0 \frac{dP_t}{dA} = -\mu_0 j_z \qquad (1)$$

where P_t is the transverse pressure, $P_t = (p + B_z^2/2\mu_0)$, and A is the partial magnetic vector potential, which has the z component only. The magnetic field can then be expressed as $B = (\partial A/\partial y, -\partial A/\partial x, B_z(x, y))$. Constant values of A describe field-line projections onto the x-y plane. The projection of the spacecraft trajectory onto the x-y plane is used as the x axis. The velocity of the structure relative to the spacecraft is determined as the HT frame velocity, by a least squares procedure (e.g., [21]). Thus, the x axis is defined to orient in the direction of $-(V_{HT} - V_{HT} \cdot \hat{z})$. The plasma thermal pressure, p, axial magnetic field, B_z, axial current density, j_z, and P_t are all functions of A alone. It is this property of the right-hand side of the GS equation that permits the reconstruction: If $P_t(A)$ and its derivative are known at one point along a field line having a particular value of A, then it is known at all points on that field line. But, as described below, $P_t(A)$ can be determined from measured plasma pressures and fields at points

along the spacecraft trajectory. Therefore the right-hand side of the GS equation is known in all regions of the *x*-*y* plane occupied by field lines that were encountered by the spacecraft, i.e., all field lines that crossed the *x* axis. In other parts of the *x*-*y* plane, the field behaviour must be recovered via suitable extrapolations of $P_t(A)$.

Since time independence of the structure is assumed, temporal variations seen by spacecraft are directly converted to spatial information along the spacecraft trajectory. As a result, all spatial parameters but *A* on the trajectory are directly be obtained from the measurements. The values of *A* along the projected spacecraft trajectory (the *x* axis) can be obtained from the measured field component, B_y, by spatial integration:

$$A(x,0) = \int \frac{\partial A}{\partial x} dx = -\int B_y(x,0) dx \qquad (2)$$

which can be converted to time integration by the relation $dx = -V_{HTx}dt$. The outcome of this integration depends on the choice of the invariant axis, from which the *x* and *y* axes can be obtained. We determine this axis by taking full advantage of multi-spacecraft information [24].

Once the function $P_t(A)$ has been determined, the integration of the GS equation proceeds as follows: measured field components, B_x and B_y, at points along the trajectory are used as spatial initial values, allowing new values to be computed by stepping away from the *x* axis in small steps, $\pm\Delta y$. As a result, a 2D distribution of *A*, $A(x, y)$, within a rectangular domain is obtained. For details about the integration procedure and validation against exact solutions of he GS equation, see the work in [20]. Validation by use of the Cluster data has been performed in [23].

Reference [24] has recently developed a simple scheme for the construction of an optimal field map and axis orientation by ingesting data from all four Cluster spacecraft as input. It contains the following elements: (1) A joint HT frame determination is made by merging data sets containing velocity measurements from the CIS/HIA instrument and magnetic field measurements from the FGM instrument onboard C1 and C3 (C2 and C4 lack CIS/HIA measurements). (2) Choice of a joint trial invariant axis is made, followed by determination of joint functions, $P_t(A)$ and $B_z(A)$. (3) Four magnetic field maps are produced, one from each spacecraft. In each map, the magnetic field from one spacecraft is used to initiate the GS integration. (4) In each map, the *A* value at each grid point is weighted by a Gaussian function of *y*, centred at the spacecraft trajectory. The resulting four *A* values are then added at each point of a joint grid, the result being a combined map of *A*, i.e., of the magnetic field projected onto the *x*-*y* plane. (5) The correlation coefficient between the field components this map predicts at points along each of the four spacecraft trajectories and the corresponding actually measured field components is calculated. It is then optimized by varying the choice of the invariant axis, the needed extrapolations of the functions $P_t(A)$ and $B_z(A)$, and the width of the Gaussian weight function. One arrives at the optimal map only after a large number of reconstructions have been performed. The optimal map no longer obeys the GS equation exactly. It accommodates deviations from the ideal model assumptions but preserves $\partial/\partial z = 0$. Once the optimum has been found, one can also generate optimal functions $p(A)$, $j_z(A) = dP_t(A)/dA$, etc., needed for the generation of maps describing the plasma pressure, *p*, axial current density, j_z, etc.

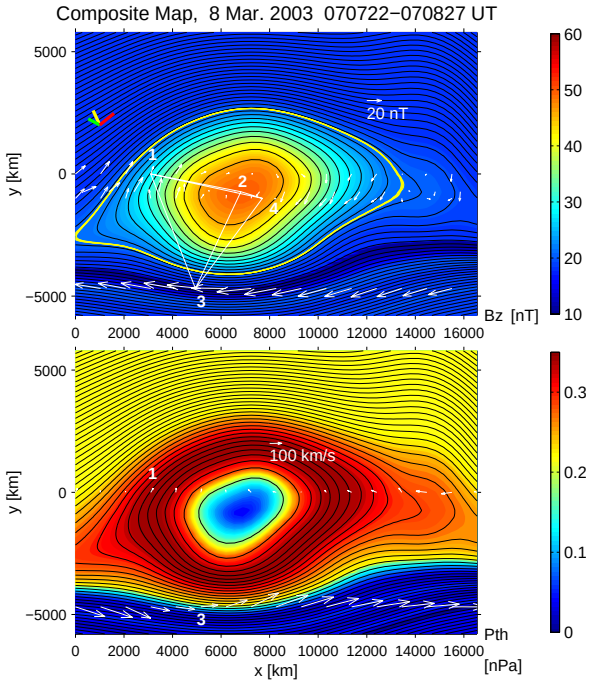

Fig. 6. Reconstructed magnetic field lines projected onto the transverse plane, with axial magnetic field (top panel) or plasma pressure (bottom panel) in colour. In the top panel, Cluster tetrahedron and measured transverse field are shown in white. The line segments in the upper left part are GSE unit vectors, *x* (red), *y* (green), and *z* (yellow), projected onto the plane. In the bottom panel, the white arrows show measured transverse velocity in the deHoffmann-Teller (HT) frame. Equatorward edge of the map is to the right with the magnetosphere on the bottom.

3.2 Structure of a flux transfer event

On 8 March 2003, when the spacecraft separation was about 5000 km and when Cluster was located near, but equatorward of, the northern cusp, the spacecraft

detected a series of flux transfer events (FTEs) [25]. Fortunately, Cluster observed some of the FTEs from both sides of the magnetopause, allowing us to reconstruct the whole structure of the FTE. Fig. 6 shows the optimal field map reconstructed for an FTE encountered at 07:07 UT, using data from all four spacecraft. The invariant axis is determined to be z = (–0.3296, –0.7434, 0.5820) in GSE. For this optimal axis, agreement between the three magnetic field components measured by Cluster and those predicted from the map at points along the four spacecraft trajectories is excellent with the correlation coefficient of 0.990 [25]. This guarantees the accuracy of the map.

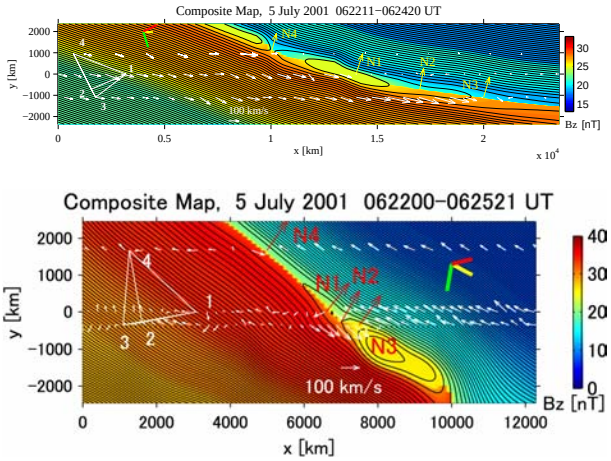

Fig. 7. Magnetic field maps for a magnetopause crossing that occurred on 5 July, 2005, 06:23 UT. The top map is reconstructed based on the data from C1 and C4, while the bottom one is based on those from C2 and C3 which crossed the boundary 30 seconds later than did C1 and C4. The colour represents the axial magnetic field, and the white arrows the measured velocity vectors, transformed into the HT frame and projected onto the plane. The yellow and red arrows anchored to the magnetopause surface are the vectors normal to the boundary, determined from the minimum variance analysis of measured magnetic field, with constraint $\langle B_n \rangle = 0$. The magnetosheath is on the upper-right side whereas the magnetosphere is on the lower-left side.

As seen in the map, the reconstructed FTE consists of a magnetic flux rope, consistent with FTE models invoking magnetic reconnection as the formation mechanism. The scale size of the flux rope in the direction normal to the magnetopause is about 1 R_E, consistent with the rough estimation reported in literature. It has a more or less round shape, although it is somewhat elongated in the direction tangential to the magnetopause. Thanks to the accurate determination of the invariant (flux rope) axis, it is demonstrated that the flux rope had a strong core field. Since such a field component cannot be produced from anti-parallel merging, it is concluded that this FTE was produced by component merging. No significant reconnection activity was present, in the sense that the measured velocity, seen in the HT frame, was very small with the Walén slope of nearly zero. The HT velocity components (V_{HT} = (–234, 51, 166) km/s in GSE) indicate that the flux rope was generally moving anti-sunward and northward. Since the IMF had a substantial –y GSE component (not shown), a subsolar reconnection X-line, if it existed, should have tilted clockwise when viewed from the sun. The orientation of the flux rope (invariant) axis as well as the direction of its motion is consistent with those expected when such a subsolar X-line leads to the FTE. It is inferred from these findings that the FTE was created through component merging that occurred much southward of the observation site, perhaps near the subsolar point. The absence of reconnection signatures implies that, by the time Cluster encountered the FTE, it nearly became a fossil structure. It appears that, during its travel to the observation site, it has deformed toward an approximate equilibrium and become a rounded shape.

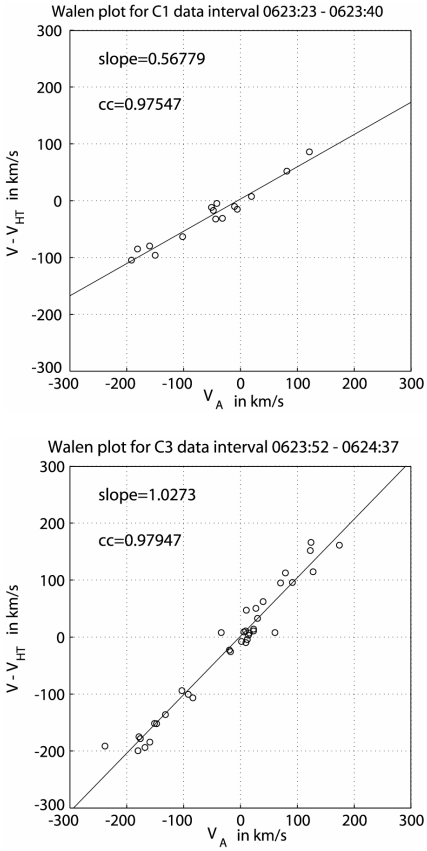

Fig. 8. The Walén plots showing relationship between the three components of the bulk velocity vectors viewed in the HT frame and the corresponding Alfvén velocity components. The top and bottom panels are for the magnetopause crossings by C1 and C3, respectively.

On the day under discussion, FTEs occurred quasi-periodically with a period of about 5 minutes. In fact, the reconstructed FTE was preceded by another FTE some 5 minutes earlier. The amount of transverse magnetic flux per unit axial length contained within the yellow field-line loop in Fig. 6 is computed to be 0.0549 Tm. This flux must have been reconnected during all, or a portion, of the 5-minute period. Then it turns out that an average reconnection electric field during the creation of the flux rope was about 0.0549/300 = 0.183 mV/m. In this calculation, we assume that the creation and activation of a reconnection *X*-line occurs equatorward of the observation site and the *X*-line then becomes inactive and is swept poleward, or perhaps starts moving first and then becomes inactive. About 5 minutes later, the process is repeated. The above estimated electric field can be converted to the reconnection rate of about 0.04, based on the components, perpendicular to the flux rope axis, of the Alfvén velocity and magnetic field on the magnetosheath side. However, since the reconnection site appears to have been located at latitudes lower than the observation point, these two values would have been larger near the reconnection site than near the observation site. Therefore the actual reconnection rate may have been somewhat lower than the above estimation.

3.3 Time evolution of magnetopause structures

By applying the Grad-Shafranov reconstruction to each of the four spacecraft, four independent field maps can be created, one from each spacecraft, allowing us to discuss temporal evolution of the structures by comparing the four maps. On 5 July, 2001, 06:23 UT, when Cluster was separated by about 2000 km and was located in the dawn flank magnetosphere, C1 and C4 crossed the magnetopause current layer nearly simultaneously while C2 and C3 crossed it nearly simultaneously but 30 seconds later than did C1 and C4 [23]. Therefore, two composite maps have been produced, one based on the C1 and C4 data, one based on the C2 and C3 data [24], the results being shown in Fig. 7. The map produced from C1 and C4 data shows the boundary of more or less tangential discontinuity-type. On the other hand, the map from C2 and C3 shows a prominent magnetic island embedded in the magnetopause and the presence of the magnetic field component penetrating from the magnetosheath into the magnetosphere near the location of the C3 crossing. Furthermore, the flow vectors seen by C3, when transformed into the HT frame, appear to show in the map that the plasma was streaming along the reconnected field lines from the magnetosheath into the magnetosphere. Comparison of the two maps suggests that the magnetopause structure has temporally evolved as a consequence of significant development of magnetopause reconnection during the interval between the crossings by C1 and C4 and by C2 and C3. Although the technique itself assumes time independence of the structure, sufficiently good agreement between the actually measured field components and those predicted from the maps [24] suggests that the maps represent, at least to some extent, what actually occurred. In addition, an independent test based on the Walén relation, satisfied for data obtained across a rotational discontinuity (RD) which, at the magnetopause, results from reconnection, supports that time evolution inferred from the comparison of the two maps was indeed present (Fig. 8). The Walén slope based on the C1 data is about 0.57 while that based on the C3 data is nearly unity. This indicates that the boundary at the time of the C3 crossing was fully of RD-type whereas that at the time of the C1 crossing was rather of tangential discontinuity-type. Furthermore, the positive sign of the Walén slope is consistent with the negative sign of the normal field component and with the expectation that the magnetosheath plasma was flowing into the magnetosphere along the field line. It appears that an incipient reconnection activity was present in the magnetopause at the moment C1 crossed the boundary and C3, which crossed the boundary 30 seconds later, detected signatures of full-blown reconnection.

Thus far, Grad-Shafranov reconstruction has been done for the recovery of the magnetic field only, but there is also a Grad-Shafranov-type equation to describe streamlines. Then, it might be possible to reconstruct a 2D map of the velocity field, for example, in and near KH vortices, from spacecraft measurements. Such a reconstruction is a future possibility.

ACKNOWLEDGEMENTS

The author thanks all the colleagues, especially, B. U. Ö. Sonnerup, M. Fujimoto, C. Hashimoto, T. K. M. Nakamura, K. Takagi, R. TanDokoro, S. E. Haaland, B. Klecker, G. Paschmann, T.-D. Phan, H. Rème, A. Balogh, M. W. Dunlop, C. J. Owen, A. Vaivads, M. André, who have contributed to the relevant work and the Cluster team for the design and successful operation of the Cluster II mission. Work at Dartmouth College was supported by NASA grant NAG5-12005. Part of the work was done while the author visited SSL, UC Berkeley. Work at TITech was performed under the auspices of a JSPS Research Fellowship for Young Scientists.

REFERENCES

1. Russell C. T. and Elphic R. C., ISEE observations of flux transfer events at the dayside magnetopause, *Geophys. Res. Lett.*, 6, 33, 1979.

2. Miura A., Anomalous transport by magnetohydrodynamic Kelvin-Helmholtz instabilities in

the solar wind-magnetosphere interaction. *J. Geophys. Res.*, 89, 801-818, 1984.

3. Hasegawa H., Fujimoto M., Phan T.-D., Rème H., Balogh A., Dunlop M. W., Hashimoto C. and TanDokoro R., Transport of solar wind into Earth's magnetosphere through rolled-up Kelvin-Helmholtz vortices, *Nature*, 430, 755-758, 2004.

4. Sckopke N. G., Paschmann G., Haerendel G., Sonnerup B. U. Ö., Bame S. J., Forbes T. G., Hones E. W., Jr. and Russell C. T., Structure of the low-latitude boundary layer. *J. Geophys. Res.* 86, 2099-2110, 1981.

5. Mitchell D. G., Kutchko F., Williams D. J., Eastman T. E., Frank L. A. and Russell C. T., An extended study of the low-latitude boundary layer on the dawn and dusk flanks of the magnetosphere., *J. Geophys. Res.* 92, 7394-7404 1987.

6. Hasegawa H., Fujimoto M., Saito Y. and Mukai, T., Dense and stagnant ions in the low-latitude boundary region under northward interplanetary magnetic field. *Geophys. Res. Lett.*, 31, L06802, 2004.

7. Terasawa T., Fujimoto M., Mukai T., et al. Solar wind control of density and temperature in the near-Earth plasma sheet: Wind/Geotail collaboration, *Geophys. Res. Lett.*, 24, 935-938, 1997.

8. Fujimoto M. and Terasawa T., Anomalous ion mixing within an MHD scale Kelvin-Helmholtz vortex, *J. Geophys. Res.*, 99, 8601-8613, 1994.

10. Nykyri K. and Otto A., Plasma transport at the magnetospheric boundary due to reconnection in Kelvin-Helmholtz vortices, *Geophys. Res. Lett.*, 28, 3565-3568, 2001.

11. Matsumoto Y. and Hoshino M., Onset of turbulence induced by a Kelvin-Helmholtz vortex, *Geophys. Res. Lett.*, 31, L02807, doi:10.1029/2003GL018195, 2004.

12. Nakamura T. K. M., Hayashi D., Fujimoto M. and Shinohara I., Decay of MHD-scale Kelvin-Helmholtz vortex, *Phys. Rev. Lett.*, 92, 145001, 2004.

13. Takagi K., Hashimoto C., Hasegawa H. and Fujimoto M., Kelvin-Helmholtz instability in a magnetotail flank-like geometry: Three-dimensional MHD simulations, *J. Geophys. Res.*, in preparation, 2005.

14. Kivelson M. G. and Chen S.-H., The magnetopause: Surface waves and instabilities and their possible dynamical consequences. in *Physics of the Magnetopause*, edited by Song P., Sonnerup B. U. Ö. and Thomsen M. F., 257-268, Geophys. Monogr. 90, American Geophysical Union, Washington, DC, 1995.

15. Fairfield D. H., Otto A., Mukai T., Kokubun S., Lepping R. P., Steinberg J. T., Lazarus A. J. and Yamamoto T., Geotail observations of the Kelvin-Helmholtz instability at the equatorial magnetotail boundary for parallel northward fields, *J. Geophys. Res.*, 105, 21159-21173, 2000.

16. Fujimoto M., Tonooka T. and Mukai T., in *Earth's low-latitude boundary layer*, edited by Newell P. T. and Onsager T., 241-251, Geophys. Monogr. 133, American Geophysical Union, Washington DC, 2003.

17. Miura A., Dependence of the magnetopause Kelvin-Helmholtz instability on the orientation of the magnetosheath magnetic field, *Geophys. Res. Lett.*, 22, 2993-2996, 1995.

18. Miura A. and Pritchett P. L., Nonlocal stability analysis of the MHD Kelvin-Helmholtz instability in a compressible plasma, *J. Geophys. Res.*, 87, 7431-7444, 1982.

19. Sundkvist D., et al. In situ multi-satellite detection of coherent vortices as a manifestation of Alfvénic turbulence, *Nature*, 436, 825-828, 2005.

20. Hau L.-N. and Sonnerup B. U. Ö., Two-dimensional coherent structures in the magnetopause: Recovery of static equilibria from single-spacecraft data, *J. Geophys. Res.*, 104, 6899-6917, 1999.

21. Khrabrov A. V. and Sonnerup B. U. Ö., DeHoffmann-Teller analysis, in *Analysis Methods for Multi-spacecraft Data*, ISSI Sci. Rep. SR-001, 221, Kluwer Acad., Norwell, Mass, 1998.

22. Sturrock P., *Plasma Physics, An introduction to the theory of astrophysical, geophysical and laboratory plasmas*, Cambridge Univ. Press, New York, 209, 1994.

23. Hasegawa H., Sonnerup B. U. Ö., Dunlop M. W., Balogh A., Haaland S. E., Klecker B., Paschmann G., Dandouras I., Lavraud B. and Rème H., Reconstruction of two-dimensional magnetopause structures from Cluster observations: Verification of method, *Ann. Geophys.*, 22, 1251-1266, 2004.

24. Hasegawa H., Sonnerup B. U. Ö., Klecker B., Paschmann G., Dunlop M. W. and Rème H., Optimal reconstruction of magnetopause structures from Cluster data, *Ann. Geophys.*, 23, 973-982, 2005.

25. Sonnerup B. U. Ö., Hasegawa H. and Paschmann G., Anatomy of a flux transfer event seen by Cluster, *Geophys. Res. Lett.*, 31, L11803, doi:10.1029/2004GL020134, 2004.